https://doi.org/10.1016/j.jmps.2019.06.017

Homogenizing interfacial shear stress via thickness gradient

Yang Gao[1,2], Haimin Yao[1,2,*]

[1] The Hong Kong Polytechnic University Shenzhen Research Institute, Shenzhen, Guangdong 518057, China

[2] Department of Mechanical Engineering, The Hong Kong Polytechnic University, Hung Hom, Kowloon, Hong Kong

[*] Corresponding author. Fax: +852 2365 4703. E-mail address: mmhyao@polyu.edu.hk (H. Yao)

Abstract:

Interfaces in bi-materials such as film-substrate systems are often subjected to shear stress due to the distinct deformation responses of two bonded materials to the external stimuli such as mechanical loading, change of temperature or humidity, or variation of internal structure induced by for example phase transformation. The distribution of such shear stress over the interface normally exhibits high concentration, which tends to initiate crack and evoke interface delamination. In such a crack propagation-mediated process of failure, the load-carrying capacity of interface has not been fully exerted as most of the interface bears little stress. To enhance the interface's resistance to delamination in bi-materials, homogenizing interfacial shear stress becomes a matter of necessity. In this paper, we propose to suppress the stress concentration on the interface by adopting films with gradient thickness. This strategy is illustrated through two typical examples of bi-material: a) a continuous film bonded on a disk-like substrate, and b) a discrete island film on a half-space substrate. For each case, theoretical solution to the optimal gradient film thickness is obtained, followed by computational and experimental validations. The results of this paper are believed to be of great and universal value to the enhancement of resistance to interfacial delamination in bi-materials.

Keywords: Stress concentration; Interface delamination; Strain misfit; Thermal expansion; Thin film

1. Introduction

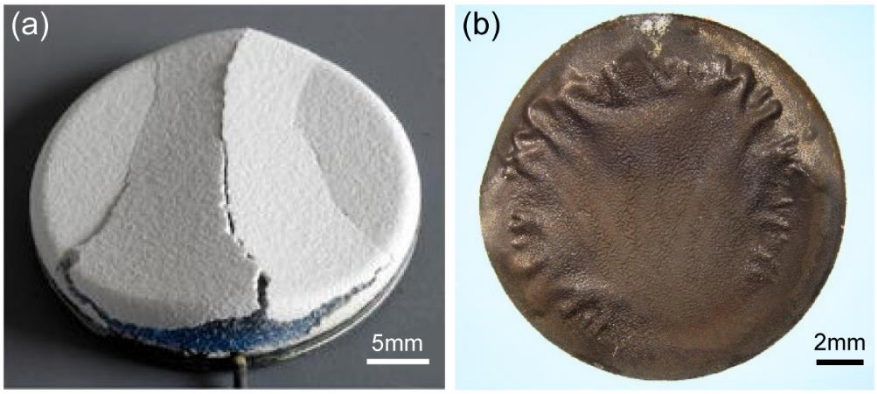

Fig. 1. (a) Ceramic thermal barrier coating delaminated from superalloy substrate after thermal cycles (Adapted with permission from Vaßen et al., 2009. Copyright 2009, Springer Nature). (b) Si-based electrode film of lithium-ion battery detached from the current collector (copper foil) after lithiation/delithiation cycles.

Bi-materials are broadly adopted in nature and engineering due to their ability to take advantage of the merits of individual constituents and to minimize their weaknesses. Different from their monolithic counterparts, bi-materials contain two materials with distinct properties. When subjected to change of external environment such as temperature and humidity or variation of internal structures due to, for example, phase transformation, the individual components may exhibit different extents of volume change, resulting in shear stress on the interface between them (Brun and Singh, 1988). Typically, such shear stress does not distribute uniformly over the interface. Instead, high stress concentration exists at the edge of interface (Akisanya and Fleck, 1997; Hein and Erdogan, 1971; Rao, 1971), where interfacial crack is apt to occur, resulting in crack propagation and subsequent interface delamination. Fig. 1(a) shows a thermal barrier coating delaminated from substrate after multiple thermal cycles (Vaßen et al., 2009) and Fig. 1(b) displays a Si-based anode film in lithium-ion battery detached from current collector after many charge-discharge cycles (Guo et al., 2019). The advent of such interfacial failure directly impairs the functionalities of the bi-material systems. Prevention of the interface delamination in bi-material systems entails mitigation of stress concentration on the interface.

Over the past few decades, a lot of efforts have been devoted to the study on interfacial stress in

bi-materials, yielding various strategies for homogenizing interfacial stress. For example, by moderating the transition slope of mechanical property across the interface between coating and substrate, functionally graded materials (FGM) were found effective in mitigating the stress concentration on the interface (Lee and Erdogan, 1994). It was reported that application of FGM could not only suppress the detachment of thermal barrier coating from substrate during thermal cycling (Wang et al., 2015) but also enhance the resistance of protective coatings to contact damages (Jitcharoen et al., 1998; Pender et al., 2001; Suresh et al., 1999). Moreover, materials with designed gradient in elasticity were also found to homogenize distribution of adhesion stress between materials and therefore enhance the adhesion strength (Yao and Gao, 2010). Recent studies on natural biomaterials revealed that gradient interlayers in natural composites play an important role in strengthening the interfaces between distinct materials (Bruet et al., 2008; Chen et al., 2012; Yao et al., 2010). In addition to FGM, size reduction is an alternative approach to mitigating stress concentration on interface. For instance, it was found that silicon island would not detach from current collector during charge-discharge cycling if its size is reduced to below a critical value around 7-10 μm (Xiao et al., 2011). Similar size effect was also found in adhesion mediated by intermolecular interactions between two contacting surfaces (Gao et al., 2005; Gao and Yao, 2004). It is noteworthy that the interfacial stress in bi-materials caused by strain misfit is shearing-dominant while the adhesion between two contacting surfaces is primarily normal traction. For the inter-surface adhesion, our previous study indicated that the traction distribution over the contacting region can also be homogenized by optimizing the profile shapes of the surfaces (Gao and Yao, 2004; Yao and Gao, 2006). Whether such strategy of shape optimization is capable of homogenizing the shear stress caused by strain misfit in bi-materials remains an open question. In this paper, theoretical analysis will be carried out to explore the feasibility of shape/geometry optimization as a novel strategy to homogenize the interfacial shear stress in bi-materials. Two sorts of bi-material systems will be considered, including continuous film on disk-like substrate and island film on half-space substrate. Our objective is to find

the optimal design of the film thickness in each case, whereby the shear stress induced by strain misfit between the film and substrate, if developed, is uniformly distributed over the whole interface.

2. Theoretical modelling

2.1 Continuous film on disk-like substrate

We first consider a bi-material consisting of a continuous thin-film coating perfectly bonded on a disk-like substrate with radius *R* and thickness t_{s}, as schematically shown in Fig. 2(a). The thickness of the film, which may not necessarily be uniform, is to be determined to achieve such an optimal scenario that uniform shear stress (τ_{de}) is developed over the interface upon strain misfit ($\varepsilon_{\mathrm{mis}}$) in between them. In other words, if such optimal thickness profile of the film, designated as $t_{\mathrm{f}}(r)$, is found and adopted, the shear stress on the interface should be uniform and equal to τ_{de}. Determination of $t_{\mathrm{f}}(r)$ can be made based on the equilibrium conditions and deformation compatibility between the film and substrate, as illustrated below. Such reverse approach for problem solving will also be applied to find the optimal thickness profile for other bi-material configurations.

Fig. 2(b) and (c) show the free body diagrams of infinitesimal elements in the substrate and film, respectively. For the substrate, equilibrium condition along the radial direction requires

$$\frac{\partial \sigma_r^{(\mathrm{s})}}{\partial r} + \frac{\sigma_r^{(\mathrm{s})} - \sigma_\theta^{(\mathrm{s})}}{r} + \frac{\tau_{\mathrm{de}}}{t_{\mathrm{s}}} = 0 \tag{1}$$

where $\sigma_r^{(\mathrm{s})}$ and $\sigma_\theta^{(\mathrm{s})}$ denote the normal stresses along the radial and circumferential directions, respectively. In Eq. (1), variables with super- or subscript ‘s’ pertain to the substrate.

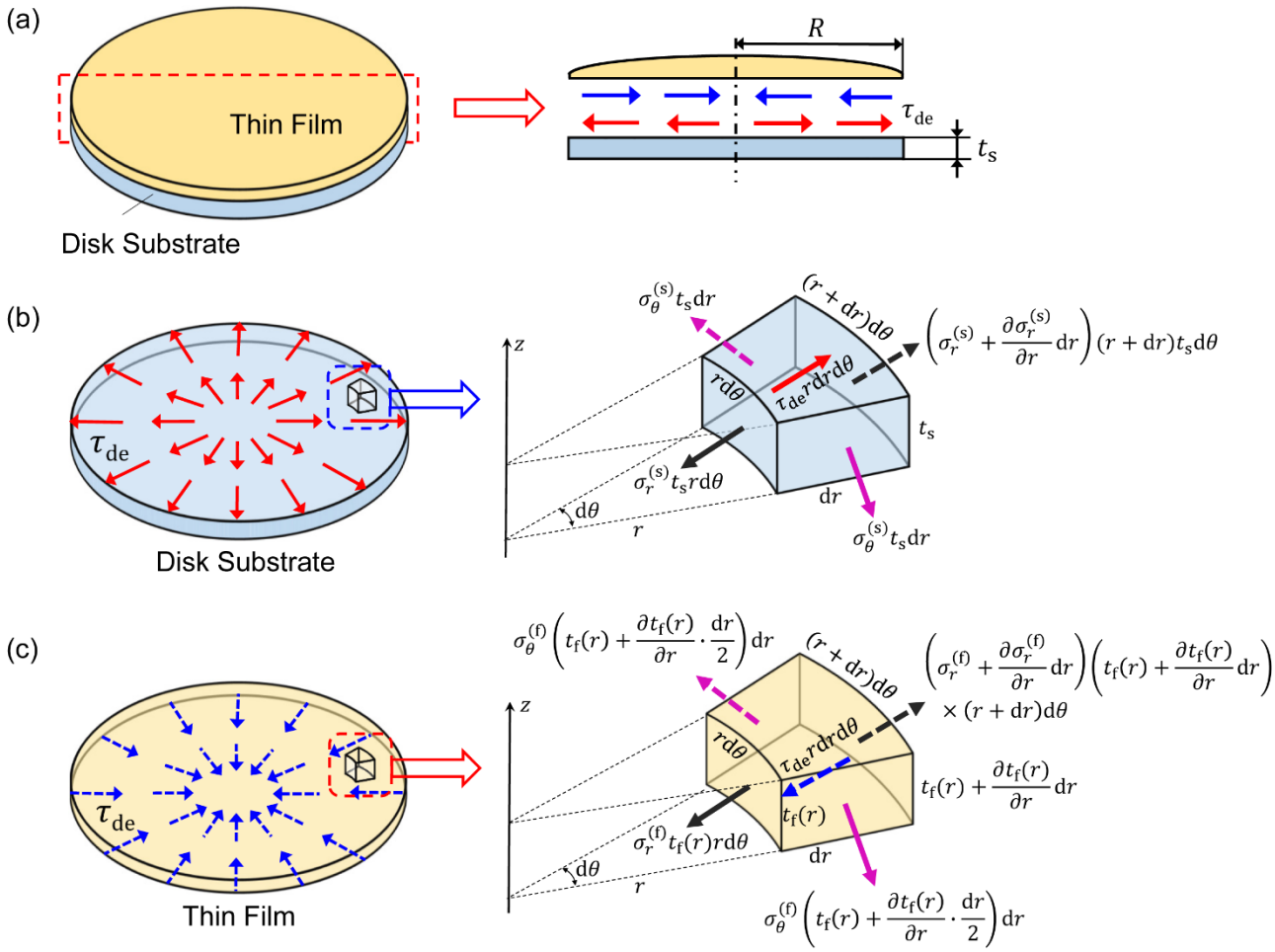

Fig. 2. (a) Schematics of a bi-material consisting of a circular film on a disk-like substrate. The nonuniform thickness of the film is to be determined so that the interfacial shear stress induced by strain misfit, if available, is uniform and equal to τ_{de}. Here, the direction of the shear stress plotted is based on the assumption that $\varepsilon_{f0} > \varepsilon_{s0}$. If $\varepsilon_{f0} < \varepsilon_{s0}$, the direction of the shear stress should be opposite or $\tau_{de} < 0$. (b, c) Free body diagrams of infinitesimal elements in the substrate and film, respectively.

For an axisymmetric problem, the normal strains in the substrate can be expressed in terms of displacement as

$$\varepsilon_r^{(s)} = \frac{\partial u_r^{(s)}}{\partial r}, \quad \varepsilon_\theta^{(s)} = \frac{u_r^{(s)}}{r} \tag{2}$$

where $u_r^{(s)}$ denotes the radial displacement of the substrate. Eq. (2) implies an important correlation between $\varepsilon_r^{(s)}$ and $\varepsilon_\theta^{(s)}$, namely

$$\varepsilon_r^{(s)} = \varepsilon_\theta^{(s)} + r \cdot \frac{\partial \varepsilon_\theta^{(s)}}{\partial r} \tag{3}$$

The total strain of the substrate contains two parts. One is the intrinsic, equiaxed strain (ε_{s0}) caused by volume change due to factors such as thermal expansion, phase transformation or moisture absorption. The other is the strain caused by stress applied on it. This part of strain can be calculated by Hooke's law if the materials are elastic as we assume here. Therefore, strains of the substrate in the radial and circumferential directions are given by

$$\varepsilon_r^{(s)} = \frac{1}{E_s}(\sigma_r^{(s)} - \nu_s\sigma_\theta^{(s)}) + \varepsilon_{s0}, \quad \varepsilon_\theta^{(s)} = \frac{1}{E_s}(\sigma_\theta^{(s)} - \nu_s\sigma_r^{(s)}) + \varepsilon_{s0} \tag{4}$$

where E_s and ν_s stand for the Young's modulus and Poisson's ratio of the substrate, respectively. In Eq. (4), the normal stress along *z* direction is neglected due to the thin thickness and free surface of the substrate. Rearrangement of Eq. (4) yields the stresses in terms of strains as

$$\sigma_r^{(s)} = \frac{E_s}{1-\nu_s^2}(\varepsilon_r^{(s)} + \nu_s\varepsilon_\theta^{(s)}) - \frac{E_s\varepsilon_{s0}}{1-\nu_s}, \quad \sigma_\theta^{(s)} = \frac{E_s}{1-\nu_s^2}(\varepsilon_\theta^{(s)} + \nu_s\varepsilon_r^{(s)}) - \frac{E_s\varepsilon_{s0}}{1-\nu_s} \tag{5}$$

Substituting Eq. (3) into Eq. (5) to eliminate $\varepsilon_r^{(s)}$ leads to

$$\sigma_r^{(s)} = \frac{E_s}{1-\nu_s}\cdot(\varepsilon_\theta^{(s)} - \varepsilon_{s0}) + \frac{E_s r}{1-\nu_s^2}\cdot\frac{\partial\varepsilon_\theta^{(s)}}{\partial r}, \quad \sigma_\theta^{(s)} = \frac{E_s}{1-\nu_s}\cdot(\varepsilon_\theta^{(s)} - \varepsilon_{s0}) + \frac{E_s\nu_s r}{1-\nu_s^2}\cdot\frac{\partial\varepsilon_\theta^{(s)}}{\partial r} \tag{6}$$

Inserting Eq. (6) into Eq. (1), the equilibrium equation can be rewritten in terms of circumferential strain $\varepsilon_\theta^{(s)}$ as

$$r\cdot\frac{\partial^2\varepsilon_\theta^{(s)}}{\partial r^2} + 3\cdot\frac{\partial\varepsilon_\theta^{(s)}}{\partial r} + \frac{\tau_{de}(1-\nu_s^2)}{E_s t_s} = 0 \tag{7}$$

Solving Eq. (7) for $\varepsilon_\theta^{(s)}$ yields

$$\varepsilon_\theta^{(s)} = -\frac{\tau_{de}(1-\nu_s^2)}{3E_s t_s}\cdot r + C_1$$

where constant C_1, according to Eq. (6) and boundary condition of $\sigma_r^{(s)}|_{r=R} = 0$, is determined as $C_1 = \varepsilon_{s0} + \frac{(2+\nu_s)(1-\nu_s)\tau_{de}R}{3E_s t_s}$. Consequently, the circumferential strain $\varepsilon_\theta^{(s)}$ is given by

$$\varepsilon_\theta^{(\mathrm{s})} = k \cdot r + b + \varepsilon_{\mathrm{s0}} \tag{8}$$

where $k \equiv -\frac{\tau_{\mathrm{de}}(1-\nu_{\mathrm{s}}{}^2)}{3E_{\mathrm{s}}t_{\mathrm{s}}}$, and $b \equiv \frac{(2+\nu_{\mathrm{s}})(1-\nu_{\mathrm{s}})\tau_{\mathrm{de}}R}{3E_{\mathrm{s}}t_{\mathrm{s}}}$.

On the other hand, for the thin film, force equilibrium along the radial direction (see Fig. 2(c) for the free body diagram) implies

$$\frac{\partial \sigma_r^{(\mathrm{f})}}{\partial r} \cdot t_{\mathrm{f}}(r) + \sigma_r^{(\mathrm{f})} \cdot \frac{\partial t_{\mathrm{f}}(r)}{\partial r} + \frac{(\sigma_r^{(\mathrm{f})} - \sigma_\theta^{(\mathrm{f})}) t_{\mathrm{f}}(r)}{r} - \tau_{\mathrm{de}} = 0 \tag{9}$$

where $\sigma_r^{(\mathrm{f})}$ and $\sigma_\theta^{(\mathrm{f})}$ represent the normal stresses along the radial and circumferential directions respectively. In Eq. (9), variables with super- or subscript 'f' pertain to the film. The opposite signs of τ_{de} in Eqs. (9) and (1) are due to the opposite direction of the shear stresses applied on the film and substrate.

Likewise, the normal stresses in the film can also be expressed in terms of circumferential strain $\varepsilon_\theta^{(\mathrm{f})}$ as

$$\sigma_r^{(\mathrm{f})} = \frac{E_{\mathrm{f}}}{1-\nu_{\mathrm{f}}} \cdot (\varepsilon_\theta^{(\mathrm{f})} - \varepsilon_{\mathrm{f0}}) + \frac{E_{\mathrm{f}} r}{1-\nu_{\mathrm{f}}{}^2} \cdot \frac{\partial \varepsilon_\theta^{(\mathrm{f})}}{\partial r}, \quad \sigma_\theta^{(\mathrm{f})} = \frac{E_{\mathrm{f}}}{1-\nu_{\mathrm{f}}} \cdot (\varepsilon_\theta^{(\mathrm{f})} - \varepsilon_{\mathrm{f0}}) + \frac{E_{\mathrm{f}} \nu_{\mathrm{f}} r}{1-\nu_{\mathrm{f}}{}^2} \cdot \frac{\partial \varepsilon_\theta^{(\mathrm{f})}}{\partial r} \tag{10}$$

where E_{f} and ν_{f} represent the Young's modulus and Poisson's ratio of the film respectively, and $\varepsilon_{\mathrm{f0}}$ is the intrinsic strain of the film caused by volume change. Assume that the film and substrate are perfectly bonded during deformation. No slip between them implies that $u_r^{(\mathrm{f})} = u_r^{(\mathrm{s})}$ or $\varepsilon_\theta^{(\mathrm{f})} = \varepsilon_\theta^{(\mathrm{s})}$ on the interface. Substituting $\varepsilon_\theta^{(\mathrm{f})} = \varepsilon_\theta^{(\mathrm{s})} = k \cdot r + b + \varepsilon_{\mathrm{s0}}$ into Eq. (10), we have

$$\sigma_r^{(\mathrm{f})} = \frac{E_{\mathrm{f}}(kr + b + \varepsilon_{\mathrm{s0}} - \varepsilon_{\mathrm{f0}})}{1-\nu_{\mathrm{f}}} + \frac{E_{\mathrm{f}} kr}{1-\nu_{\mathrm{f}}{}^2}, \quad \sigma_\theta^{(\mathrm{f})} = \frac{E_{\mathrm{f}}(kr + b + \varepsilon_{\mathrm{s0}} - \varepsilon_{\mathrm{f0}})}{1-\nu_{\mathrm{f}}} + \frac{E_{\mathrm{f}} \nu_{\mathrm{f}} kr}{1-\nu_{\mathrm{f}}{}^2} \cdot \tag{11}$$

Defining strain misfit between the film and substrate as $\varepsilon_{\mathrm{mis}} \equiv \varepsilon_{\mathrm{f0}} - \varepsilon_{\mathrm{s0}}$, Eq. (11) thus can be rewritten as

$$\sigma_r^{(\mathrm{f})} = \frac{E_{\mathrm{f}}(kr + b - \varepsilon_{\mathrm{mis}})}{1-\nu_{\mathrm{f}}} + \frac{E_{\mathrm{f}} kr}{1-\nu_{\mathrm{f}}{}^2}, \quad \sigma_\theta^{(\mathrm{f})} = \frac{E_{\mathrm{f}}(kr + b - \varepsilon_{\mathrm{mis}})}{1-\nu_{\mathrm{f}}} + \frac{E_{\mathrm{f}} \nu_{\mathrm{f}} kr}{1-\nu_{\mathrm{f}}{}^2} \cdot \tag{12}$$

From Eq. (12), it is easy to see that the radial normal stress $\sigma_r^{(f)}$ in the thin film increases linearly from the center to the edge. This distribution of the normal stress is quite different from the uniform-thickness case, in which the radial normal stress is almost uniform along the radial direction. For the gradient thin film, therefore, failure such as fracture or buckling is prone to happen near the edge.

Inserting Eq. (12) into Eq. (9), the equilibrium equation becomes

$$\frac{\partial t_f(r)}{\partial r}+\frac{3k\cdot t_f(r)}{(2+\nu_f)kr+(b-\varepsilon_{mis})(1+\nu_f)}-\frac{\tau_{de}(1-\nu_f^{\,2})/E_f}{(2+\nu_f)kr+(b-\varepsilon_{mis})(1+\nu_f)}=0 \tag{13}$$

Solving Eq. (13) for $t_f(r)$ gives rise to

$$t_f(r)=C_2\left[(2+\nu_f)kr+(b-\varepsilon_{mis})(1+\nu_f)\right]^{-\frac{3}{2+\nu_f}}+\frac{\tau_{de}(1-\nu_f^{\,2})}{3kE_f}$$

where C_2 is a constant to be determined. Stress-free condition at the edge of the film requires

$$\sigma_r^{(f)}|_{r=R}=\frac{E_f}{1-\nu_f}\cdot\left[\frac{(1-\nu_s)\tau_{de}R}{3E_st_s}-\varepsilon_{mis}\right]-\frac{\tau_{de}E_fR(1-\nu_s^{\,2})}{3E_st_s(1-\nu_f^{\,2})}=0 \tag{14}$$

It can be demonstrated that the condition of Eq. (14) is unrealistic and cannot be satisfied (see Appendix A). Alternatively, a weak-form boundary condition is thus proposed that the radial force per unit length $\sigma_r^{(f)}t_f$ or t_f, rather than stress $\sigma_r^{(f)}$, vanishes at the edge r=R. In doing so, constant C_2 is determined as

$$C_2=-\frac{\tau_{de}(1-\nu_f^{\,2})}{3kE_f}\cdot\left[(2+\nu_f)kR+(b-\varepsilon_{mis})(1+\nu_f)\right]^{\frac{3}{2+\nu_f}}$$

Eventually, the analytical solution to the optimal thickness profile is given by

$$t_f(r)=\frac{E_st_s(1-\nu_f^{\,2})}{E_f(1-\nu_s^{\,2})}\left\{\left[\frac{(\nu_f+2)(1-\nu_s^{\,2})+\left[\frac{3E_st_s\varepsilon_{mis}}{R\tau_{de}}-(\nu_s+2)(1-\nu_s)\right](\nu_f+1)}{(\nu_f+2)(1-\nu_s^{\,2})\cdot\frac{r}{R}+\left[\frac{3E_st_s\varepsilon_{mis}}{R\tau_{de}}-(\nu_s+2)(1-\nu_s)\right](\nu_f+1)}\right]^{\frac{3}{\nu_f+2}}-1\right\}. \tag{15}$$

By taking $E_f=100$ GPa, $\nu_f=0.3$, $E_s=200$ GPa, $\nu_s=0.25$, $R=10$ mm, $t_s=10$ μm, $\varepsilon_{mis}=$

1% and $\tau_{de} = 1$ MPa, the thickness profile of the nonuniform film given above is plotted in Fig. 3(a), which appears like a cone.

Finite element analysis was carried out to examine the shear stress developed on the interface between a film with thickness given by Eq. (15) and a disk-like substrate. In our simulation, both the film and substrate were depicted as linear elastic materials, while the interface between them was modelled by zero-thickness cohesive element. The intrinsic strain was equivalently implemented by thermal expansion with expansion coefficient misfit between the film and substrate taken as ε_{mis}. The simulated results at different levels of strain misfit, which were implemented by applying different temperature increments, are displayed in Fig. 3(b). As expected, the shear stress, except that in the vicinity of the central symmetric point, displays a uniform distribution over the interface. The magnitude of the uniform shear stress is linearly proportional to the applied strain misfit with slope being $\tau_{de}/\varepsilon_{mis}$, which stands for the shear stress developed by unit strain misfit.

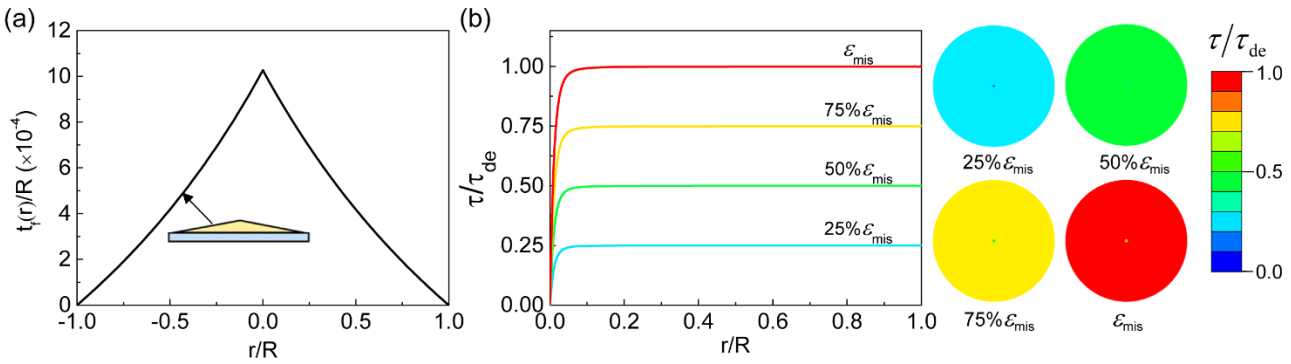

Fig. 3. (a) Profile of the optimal gradient film thickness. (b) The simulated shear stress field on the interface between the thin film and substrate at different degrees of strain misfit. Parameters adopted: $E_f = 100$ GPa, $\nu_f = 0.3$, $E_s = 200$ GPa, $\nu_s = 0.25$, $R = 10$ mm, $t_s = 10$ μm, $\varepsilon_{mis} = 1\%$ and $\tau_{de} = 1$ MPa. The stiffness of the cohesive interface is taken as 100 GPa/mm.

It is worth pointing out that in the above analysis, the bending effect has not been taken into account since in many cases of bi-material, such as the electrode-current collector system in lithium-ion batteries, the out-of-plane deformation is firmly constrained. But for free-standing bi-materials, the strain misfit would result in curved configuration which in return affects the interfacial shear stress

distribution. In that case, the above solution to the optimal gradient thickness for homogenizing the shear stress may not be applicable anymore. Separate study is needed to shed light on the effect of bending on the interfacial shear stress distribution.

2.2 Island film on half-space substrate

Above solution to the optimal thickness profile applies to bi-material systems in which the film continuously and fully covers the substrate. In some circumstances, however, film and substrate may have quite distinct sizes in plane and/or thickness. Examples include discontinuous wear-resistant coating on cutting tools (Antonyuk et al., 2007; Ramachandra and Ovaert, 2000; Soroka et al., 2011; Volosova et al., 2016) and silicon islands on current collector in electrodes of lithium-ion batteries (Haftbaradaran et al., 2012a; Haftbaradaran et al., 2012b; Soni et al., 2011; Xiao et al., 2011). To extend our conception of stress homogenization to these cases, we keep on exploring the optimal thickness profile for an island film attached on a half-space substrate, as schematically shown in Fig. 4(a). Similarly, we designate the optimal thickness profile of the film as $t_{\mathrm{f}}(r)$, whereby uniform shear stress τ_{de} is developed over the interface when strain misfit of $\varepsilon_{\mathrm{mis}}$ takes place between the film and substrate. The determination of function $t_{\mathrm{f}}(r)$ is made as follows.

For the half-space substrate, when a uniform shear stress with magnitude of τ_{de} is applied over a circular region of radius R (see Fig. 4(b)), the resulting radial displacement in this region is given by (Johnson, 1987)

$$u_r^{(\mathrm{s})}(r)=\frac{4R^2\tau_{\mathrm{de}}(1-\nu_{\mathrm{s}}{}^2)}{E_{\mathrm{s}}\pi r}\int_0^{r/R}\frac{\lambda^2\cdot[\ln(1+\sqrt{1-\lambda^2})-\ln\lambda]}{\sqrt{(r/R)^2-\lambda^2}}\mathrm{d}\lambda$$

where E_{s} and ν_{s} represent the Young's modulus and Poisson's ratio of the substrate, respectively. Here, super- and subscript 's' pertain to the substrate. The corresponding circumferential strain is given by

$$\tilde{\varepsilon}_\theta^{(\mathrm{s})} = \frac{u_r^{(\mathrm{s})}}{r} = \frac{4R^2\tau_{\mathrm{de}}(1-\nu_{\mathrm{s}}^{\,2})}{E_{\mathrm{s}}\pi r^2}\int_0^{r/R}\frac{\lambda^2\cdot[\ln(1+\sqrt{1-\lambda^2})-\ln\lambda]}{\sqrt{(r/R)^2-\lambda^2}}\mathrm{d}\lambda$$

Thus, the total circumferential strain, including the intrinsic portion, can be expressed as

$$\varepsilon_\theta^{(\mathrm{s})} = \varepsilon_{\mathrm{s0}} + \tilde{\varepsilon}_\theta^{(\mathrm{s})} = \varepsilon_{\mathrm{s0}} + \frac{4R^2\tau_{\mathrm{de}}(1-\nu_{\mathrm{s}}^{\,2})}{E_{\mathrm{s}}\pi r^2}\int_0^{r/R}\frac{\lambda^2\cdot[\ln(1+\sqrt{1-\lambda^2})-\ln\lambda]}{\sqrt{(r/R)^2-\lambda^2}}\mathrm{d}\lambda \tag{16}$$

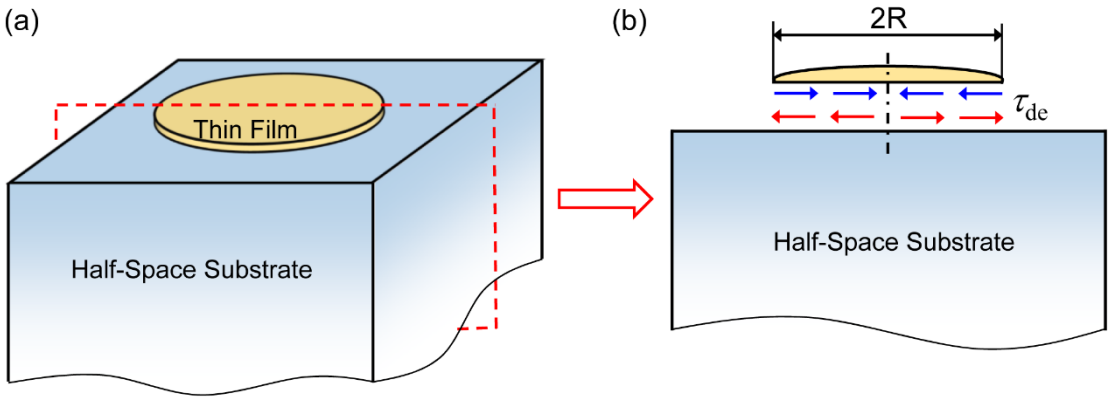

Fig. 4. (a) Schematics of a bi-material consisting of a circular island film on a half-space substrate. The thickness of the film is to be optimized so that the interfacial shear stress induced by strain misfit, if available, is uniform and equal to τ_{de} as shown in (b).

For the circular island film, Eqs. (9) and (10) still apply. We therefore have

$$\frac{\partial\sigma_r^{(\mathrm{f})}}{\partial r}\cdot t_{\mathrm{f}}(r) + \sigma_r^{(\mathrm{f})}\cdot\frac{\partial t_{\mathrm{f}}(r)}{\partial r} + \frac{(\sigma_r^{(\mathrm{f})}-\sigma_\theta^{(\mathrm{f})})t_{\mathrm{f}}(r)}{r} - \tau_{\mathrm{de}} = 0 \tag{17}$$

$$\sigma_r^{(\mathrm{f})} = \frac{E_{\mathrm{f}}}{1-\nu_{\mathrm{f}}}\cdot(\varepsilon_\theta^{(\mathrm{f})}-\varepsilon_{\mathrm{f0}}) + \frac{E_{\mathrm{f}}r}{1-\nu_{\mathrm{f}}^{\,2}}\cdot\frac{\partial\varepsilon_\theta^{(\mathrm{f})}}{\partial r},\quad \sigma_\theta^{(\mathrm{f})} = \frac{E_{\mathrm{f}}}{1-\nu_{\mathrm{f}}}\cdot(\varepsilon_\theta^{(\mathrm{f})}-\varepsilon_{\mathrm{f0}}) + \frac{E_{\mathrm{f}}\nu_{\mathrm{f}}r}{1-\nu_{\mathrm{f}}^{\,2}}\cdot\frac{\partial\varepsilon_\theta^{(\mathrm{f})}}{\partial r} \tag{18}$$

Assuming that the island film and substrate are perfectly bonded during deformation, we have $\varepsilon_\theta^{(\mathrm{f})} = \varepsilon_\theta^{(\mathrm{s})} = \tilde{\varepsilon}_\theta^{(\mathrm{s})} + \varepsilon_{\mathrm{s0}}$. Substitution of this relationship into Eq. (18) to eliminate $\varepsilon_\theta^{(\mathrm{f})}$ gives

$$\sigma_r^{(\mathrm{f})} = \frac{E_{\mathrm{f}}}{1-\nu_{\mathrm{f}}}\cdot(\tilde{\varepsilon}_\theta^{(\mathrm{s})}-\varepsilon_{\mathrm{mis}}) + \frac{E_{\mathrm{f}}r}{1-\nu_{\mathrm{f}}^{\,2}}\cdot\frac{\partial\tilde{\varepsilon}_\theta^{(\mathrm{s})}}{\partial r},\quad \sigma_\theta^{(\mathrm{f})} = \frac{E_{\mathrm{f}}}{1-\nu_{\mathrm{f}}}\cdot(\tilde{\varepsilon}_\theta^{(\mathrm{s})}-\varepsilon_{\mathrm{mis}}) + \frac{E_{\mathrm{f}}\nu_{\mathrm{f}}r}{1-\nu_{\mathrm{f}}^{\,2}}\cdot\frac{\partial\tilde{\varepsilon}_\theta^{(\mathrm{s})}}{\partial r} \tag{19}$$

where $\varepsilon_{\mathrm{mis}} \equiv \varepsilon_{\mathrm{f0}} - \varepsilon_{\mathrm{s0}}$. Substituting Eq. (19) into (17) yields

$$\frac{\partial t_{\mathrm{f}}(r)}{\partial r} + P(r)\cdot t_{\mathrm{f}}(r) = Q(r) \tag{20}$$

where

$$P(r)=\frac{3\cdot\dfrac{\partial\tilde{\varepsilon}_\theta^{(\mathrm{s})}}{\partial r}+r\cdot\dfrac{\partial^2\tilde{\varepsilon}_\theta^{(\mathrm{s})}}{\partial r^2}}{(1+\nu_\mathrm{f})\tilde{\varepsilon}_\theta^{(\mathrm{s})}+r\cdot\dfrac{\partial\tilde{\varepsilon}_\theta^{(\mathrm{s})}}{\partial r}-\varepsilon_\mathrm{mis}(1+\nu_\mathrm{f})},\quad Q(r)=\frac{\tau_\mathrm{de}(1-\nu_\mathrm{f}^{\,2})/E_\mathrm{f}}{(1+\nu_\mathrm{f})\tilde{\varepsilon}_\theta^{(\mathrm{s})}+r\cdot\dfrac{\partial\tilde{\varepsilon}_\theta^{(\mathrm{s})}}{\partial r}-\varepsilon_\mathrm{mis}(1+\nu_\mathrm{f})}.$$

The mathematical complexity of Eq. (20) implies the difficulty of finding the analytical solution to the function $t_\mathrm{f}(r)$. Finite difference method was adopted to solve the equation numerically. As the stress-free condition that $\sigma_r^{(\mathrm{f})}=0$ at the edge (r=R) can be proved unrealistic (see Appendix B), alternative weak-form boundary condition of $\sigma_r^{(\mathrm{f})}t_\mathrm{f}=0$ or $t_\mathrm{f}=0$ at r=R is adopted to determine the profile function $t_\mathrm{f}(r)$. If we take $E_\mathrm{f}=100$ GPa, $\nu_\mathrm{f}=0.3$, $E_\mathrm{s}=200$ GPa, $\nu_\mathrm{s}=0.25$, $R=10$ mm, $\varepsilon_\mathrm{mis}=1\%$ and $\tau_\mathrm{de}=1$ MPa, the calculated solution to the thickness profile of the optimal island film is displayed in Fig. 5(a). Likewise, finite element analysis was carried out to examine the shear stress distribution over the interface between an island film with thickness profile shown in Fig. 5(a) and a substrate of sufficiently large size. As shown in Fig. 5(b), the shear stress on the interface, except that in the area very close to the symmetric center, keeps uniform under different levels of strain misfit with magnitude growing at a rate of $\tau_\mathrm{de}/\varepsilon_\mathrm{mis}$. Therefore, the validity of the numerical result is confirmed.

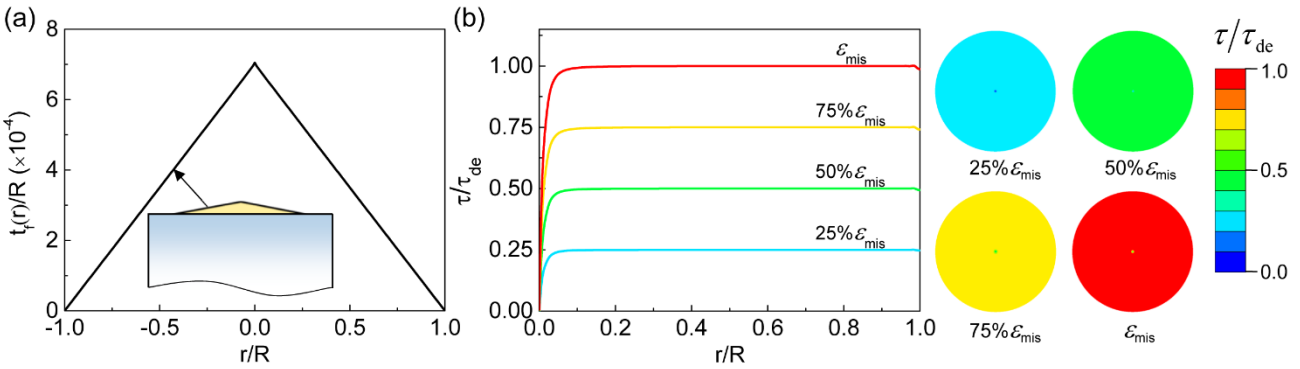

Fig. 5. (a) Profile of the optimal nonuniform island film thickness. (b) The simulated shear stress field on the interface between the thin film and substrate at different degrees of strain misfit. Parameters adopted: $E_\mathrm{f}=100$ GPa, $\nu_\mathrm{f}=0.3$, $E_\mathrm{s}=200$ GPa, $\nu_\mathrm{s}=0.25$, $R=10$ mm, $\varepsilon_\mathrm{mis}=1\%$ and $\tau_\mathrm{de}=1$ MPa. The stiffness of the cohesive interface is taken as 100 GPa/mm.

It is observed from Fig. 5(a) that $t_\mathrm{f}(r)$ is very close to a linear function, implying the possible

presence of a linear approximation of $t_f(r)$. It can be demonstrated that if the nondimensional parameter $\varphi = \frac{E_s \varepsilon_{mis}(1+\nu_f)}{\tau_{de}(1-\nu_s^2)}$ is large enough, the thickness profile can be approximated by a linear function as (see Appendix C)

$$t_f(r) \cong \frac{\tau_{de}(1-\nu_f)}{\varepsilon_{mis} E_f}(R-r), \tag{21}$$

which describes a cone with included angle of $2\arctan\frac{E_f \varepsilon_{mis}}{\tau_{de}(1-\nu_f)}$. It is worth noting that the ratio $\tau_{de}/\varepsilon_{mis}$ in Eq. (21) also represents the interfacial shear stress developed by unit strain misfit. The validity of this approximation and its dependence on the nondimensional parameter φ were examined by finite element analysis. Fig. 6 displays the linear approximations of the optimal thickness profiles (namely Eq. (21)) for cases with different φ and the corresponding calculated shear stress distribution on the interface under strain misfit of ε_{mis}. As can be observed, if φ is on the order of magnitude of 10^3 or above, the stress field, except that in the vicinity of the central symmetric point, is uniform throughout the interface. When φ is on the order of magnitude of 10^2 or below, the stress field exhibits nonuniform distribution, implying the significant deviation of Eq. (21) from the actual solution to the optimal thickness.

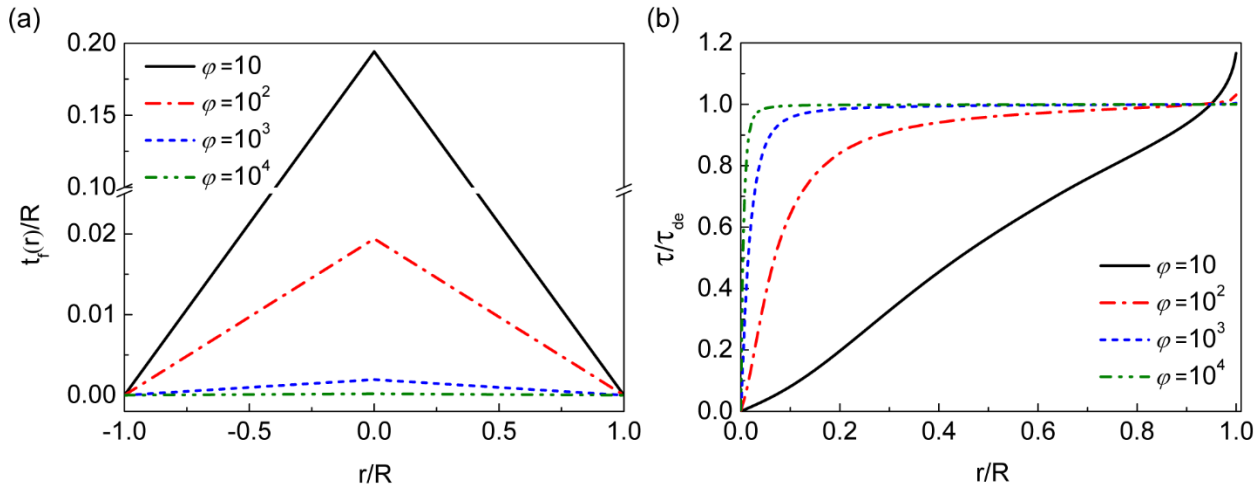

Fig. 6. (a) Linear approximations of the optimal thickness profiles of island film for different φ. (b) The simulated shear stress field on the interface between the island film and substrate under the strain misfit ε_{mis}. Here, $E_f = 100$ GPa, $\nu_f = 0.3$, $E_s = 200$ GPa, $\nu_s = 0.25$, $R = 10$ mm, $\varepsilon_{mis} = 1\%$ and $\tau_{de} = 0.277, 2.773, 27.733,$ or 277.333 MPa. The stiffness of cohesive interface is taken as 100

GPa/mm.

2.3 Solutions to plane-strain configurations

In addition to the above axisymmetric configurations of bi-material, thin film strips bonded on substrate have also been widely used. Typical examples include metal conduction lines in microelectronic devices (Yu and Hutchinson, 2003) and optical waveguides in photonic devices (Yu and Hutchinson, 2003). To tackle the stress concentration problem in these configurations, we further extend our study to the configuration of a thin film strip attached on a substrate (see Table.1), where plane-strain condition prevails. Similarly, we aim to find the optimal thickness profile $t_{\mathrm{f}}(x)$ for the film strips, whereby a uniform shear stress field τ_{de} will be developed on the interface when strain misfit $\varepsilon_{\mathrm{mis}}$ takes place between them.

The approach to solving $t_{\mathrm{f}}(x)$ for the plane-strain configurations is similar to that applied in the preceding axisymmetric cases. Firstly, we need to determine the strain field of the substrate $\varepsilon_x^{(\mathrm{s})}$ which can be obtained based on equilibrium conditions or by referring to existing solutions in contact mechanics (Johnson, 1987). Then with the assumption that film and substrate are perfectly bonded, the strain field in the film ($\varepsilon_x^{(\mathrm{f})}$) and substrate ($\varepsilon_x^{(\mathrm{s})}$) should be equal. Knowing the strain field in the film $\varepsilon_x^{(\mathrm{f})}$, the film thickness $t_{\mathrm{f}}(x)$ can be determined based on equilibrium conditions. This method was repeatedly used here to determine the optimal film thickness under different plane-strain configurations.

Table 1 lists the analytical solutions to $t_{\mathrm{f}}(x)$ (in normalized form) for different plane-strain configurations. Case (a) describes a bi-material consisting of a strip film and substrate which have comparable sizes in plane and thickness. The film and substrate have different intrinsic deformation. In case (b), no intrinsic deformation occurs in the film, while the substrate deforms along transverse direction under uniaxial loading. Both cases (c) and (d) depict a strip film attached on a half-space substrate. In case (c), the film and half-space substrate have different intrinsic deformation, while in case (d) only the substrate deforms due to the external mechanical loading along the transverse direction. For each case, the theoretical solution to the optimal thickness of the film was well verified

via finite element simulation, as shown in Table 1. It is worth pointing out that the solutions for cases (c) and (d) provided in Table.1 are the asymptotic solutions under conditions as indicated.

Table 1. The optimal film thickness for different plane-strain configurations

Plane-strain configuration	Analytical solution to $t_f(x)$	Profile of optimal thickness of the film and shear stress distribution*
(a) 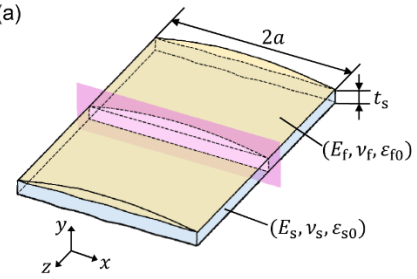	$\bar{t}_f(x/a) = \frac{t_f(x)}{a} \cdot \frac{E_f[(1+\nu_f)\varepsilon_{f0} - (1+\nu_s)\varepsilon_{s0}]}{\tau_{de}(1-\nu_f^2)}$ $= \frac{1}{\frac{1}{1-x/a} - \frac{a\tau_{de}(1-\nu_s^2)}{E_s t_s[(1+\nu_f)\varepsilon_{f0} - (1+\nu_s)\varepsilon_{s0}]}}$	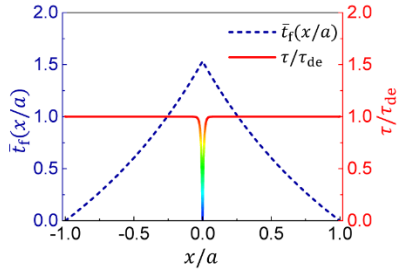
(b) 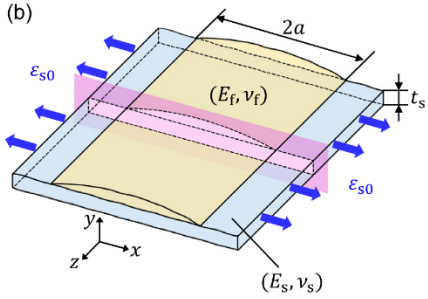	$\bar{t}_f(x/a) = \frac{t_f(x)}{a} \cdot \frac{\varepsilon_{s0}E_f}{(-\tau_{de})(1-\nu_f^2)}$ $= \frac{1}{\frac{1}{1-x/a} + \frac{a\tau_{de}(1-\nu_s^2)}{E_s t_s \varepsilon_{s0}}}$	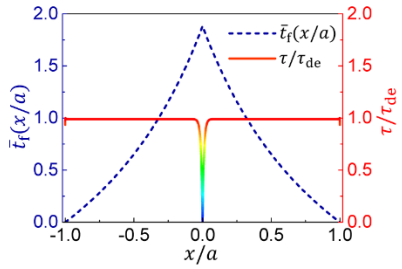
(c) 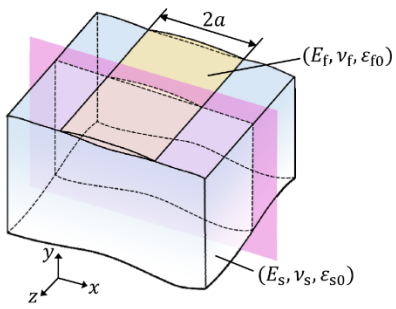	Asymptotic solution to $\bar{t}_f(x/a)$ as $\frac{E_s[(1+\nu_f)\varepsilon_{f0}-(1+\nu_s)\varepsilon_{s0}]}{\tau_{de}(1-\nu_s^2)} \to \infty$: $\bar{t}_f(x/a) = \frac{t_f(x)}{a} \cdot \frac{E_f[(1+\nu_f)\varepsilon_{f0} - (1+\nu_s)\varepsilon_{s0}]}{\tau_{de}(1-\nu_f^2)}$ $\cong 1 - x/a$	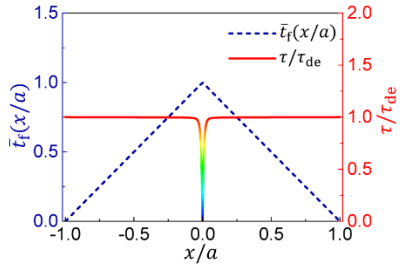
(d) 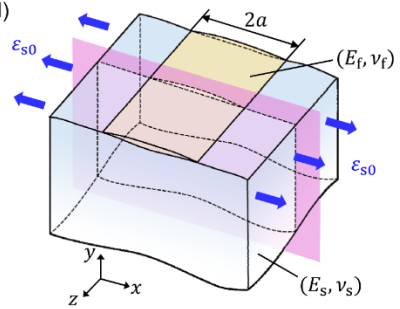	Asymptotic solution to $\bar{t}_f(x/a)$ as $\frac{E_s\varepsilon_{s0}}{(-\tau_{de})(1-\nu_s^2)} \to \infty$: $\bar{t}_f(x/a) = \frac{t_f(x)}{a} \cdot \frac{\varepsilon_{s0}E_f}{(-\tau_{de})(1-\nu_f^2)}$ $\cong 1 - x/a$	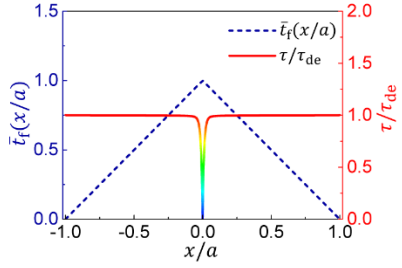

*Profiles of optimal thickness of the film and corresponding simulation results are taken as examples with parameters adopted as follows: $E_f = 100$ GPa, $\nu_f = 0.3$, $E_s = 200$ GPa, $\nu_s = 0.25$, $a = 10$ mm, $t_s = 10$ μm, $\varepsilon_{s0} = 1\%$, $\varepsilon_{f0} = 2\%$, $\tau_{de} = 1$ MPa for (a)(c) and $\tau_{de} = -1$ MPa for (b)(d). The cohesive interface stiffness is taken as 100 GPa/mm.

3. Experimental validation

The preceding section gives the theoretical solutions to the optimal film thickness, whereby the shear stress field on the interface of bi-material is expected to be homogenized. In this section, experimental validation of this strategy was carried out. For the sake of simplicity, we choose the

plane-strain configuration displayed in Table.1(b) for illustration, namely, a substrate expands by strain ε_{s0} along x direction under a tensile loading σ_t. Based on Hooke's law and plane-strain condition, it is easy to demonstrate that $\varepsilon_{s0} = \frac{\sigma_t(1-\nu_s^2)}{E_s}$. Thus, the optimal film thickness can be rewritten in terms of σ_t as

$$t_f(x) = \frac{t_s(1-\nu_f^2)E_s/(1-\nu_s^2)E_f}{t_s\sigma_t/(x-a)\tau_{de}-1}. \tag{22}$$

To verify this solution to the optimal thickness, acrylonitrile butadiene styrene (ABS) and Al 6061-T6 were employed to produce film-substrate bi-materials. Taking $E_f = 2.2$ GPa, $\nu_f = 0.35$ (Ingrole et al., 2017), and $E_s = 68.9$ GPa, $\nu_s = 0.33$ (Kurniawan and Ko, 2013), $|\sigma_t/\tau_{de}| = 300$, $a = 30$ mm and $t_s = 5$ mm, the optimal film thickness can be calculated as displayed in Fig. 7(a). The gradient films were manufactured by 3D printing (μPrint SE Plus, Stratasys) using ABS (ABSplus-P430, Stratasys) and adhered onto the substrate surface with all-purpose superglue (Aron Alpha), as schematically shown in Fig. 7(b). For comparison, uniform films were also prepared with thickness profile shown in Fig. 7(a). Since direct measurement of stress field is challenging, the shear strain field, which is believed proportional to the shear stress filed for elastic deformation, was measured instead by using Digital Image Correlation technology (DIC) (Pan et al., 2009). For this purpose, before the experiment the side surfaces to be tracked were spray-pained with uniform random speckle pattern as schematically shown in Fig. 7(b). Tensile loading was then applied on the substrate with a universal testing machine (GP-TS2000M, Gopoint) at a crosshead speed of 2 mm/min. During deformation, digital images of speckle pattern were captured every 10 s using a digital camera (Sony α57) with resolution of 31-33 pixels/mm. Based on the obtained images, DIC analysis was carried out with Ncorr (Blaber et al., 2015), an open-source subset-based 2D DIC software package, to gain the shear strain field.

Fig. 7(c) shows the obtained shear strain field of the side surface under tensile loading of σ_t = 173.3 MPa, from which the shear strain along the interface was extracted and displayed in Fig. 7(d).

As expected, in the case with gradient film, the shear strain field developed along the bonded interface is almost uniform despite of some fluctuations. In contrast, in the control case with uniform-thickness film, severe strain concentration occurred at interface edge. It is confirmed that gradient film thickness in bi-materials could effectively homogenize the shear stress on the interface, and consequently improve their resistance to interfacial crack initiation. As the shear stress along the interface is homogenized, the whole interface, upon sufficiently high loading, would fail simultaneously if the interfacial strength is uniform everywhere. In reality, however, interfacial crack would be firstly initiated at the weakest point on the interface. Once the crack is initiated, the distribution of shear stress along the interface is changed and becomes non-uniform. After that, gradient thickness would not be too much different from a uniform counterpart in resisting crack propagation.

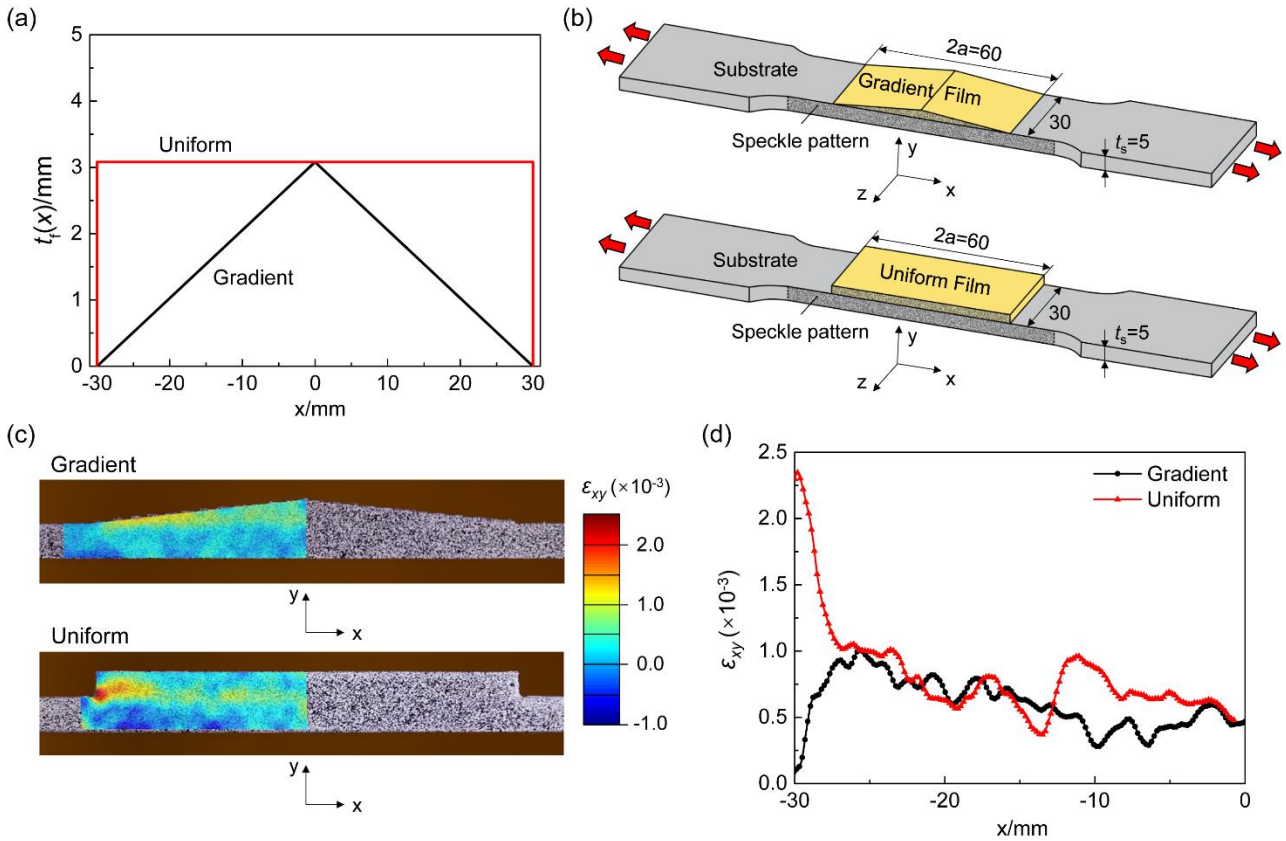

Fig. 7. (a) Thickness profiles of the optimal gradient film and uniform control. (b) Schematics of the experimental setups (units: mm). (c) Shear strain field (ε_{xy}) on the side surface under a tensile loading $\sigma_t = 173.3$ MPa, which was obtained by DIC analysis using software Nccor with the subset size, subset spacing and strain radius being taken as 40 pixels, 1 pixel and 15 pixels, respectively. (d) Shear

strain (ε_{xy}) distribution along the interface between film and substrate under tensile loading $\sigma_{\mathrm{t}} = 173.3$ MPa.

4. Conclusion and discussion

In summary, in this paper we proposed to homogenize interfacial shear stress in bi-materials caused by strain misfit via thickness gradient. The solutions to the gradient thickness were obtained and the effectiveness of this strategy was demonstrated based on two typical bi-material systems: continuous film on disk-like substrate and island film on half-space substrate. The results in this paper are believed to be of great value to the enhancement of resistance to interface delamination, either instant or fatigue-caused, in a variety of thin films such as thermal barrier coating (Choi et al., 1999), wear-resistant coating (Qin et al., 2009), electrode film on current collector in batteries (Basu et al., 2018) and discontinuous islands coating on biomedical devices (Schaldach and Kranz, 2004). In practice, however, there might be some occasions in which the film thickness has to be uniform due to some specific functional requirement. Under such kind of circumstances, adopting gradient stiffness (*i.e.*, elastic modulus) would be an alternative strategy, because it is easy to see from our theoretical solutions above that gradient stiffness actually plays an equivalent role in homogenizing the interfacial shear stress distribution as gradient thickness does. Different from the traditional FGMs with stiffness gradient along the thickness direction, here stiffness varies in an appropriate manner along the direction parallel to the interface. Implementation of such gradient stiffness, however, is more challenging in manufacturing compared to that of the gradient thickness.

Another potential contribution of our results may lie in the measurement of shear strength of interfaces between coating and substrate or fiber and matrix in composites. Traditionally, shear test (Zhu et al., 1999) or pull-out test (Valadez-Gonzalez et al., 1999) is adopted to characterize the shear strength which is often taken as the pull-off force divided by the contact area. Such method tends to underestimate the shear strength because of the presence of stress concentration on the interface (Era et al., 1998; Piggott, 1997). If a uniform shear stress distribution is achieved with the application of the proposed strategy of gradient thickness, more accurate measurement of shear strength is expected.

However, limitations remain present in our work. First, our analysis assumed that both the film and substrate are elastic. This might not be always the case as the mechanical properties of a material may change in service as exemplified by the electrode of lithium-ion battery in process of lithiation and delithiation (Shenoy et al., 2010). Additionally, in our theoretical analysis for determining the optimal gradient thickness of film, the possible buckling of the film caused by compressive stress has not be considered. Further investigations are needed to take these issues into account.

Acknowledgment

Supports for this work from the Natural Science Foundation of China (Grant No. 11772283), General Research Fund (GRF) of Hong Kong RGC (PolyU 152193/14E, PolyU 152064/15E), Central Research Grant from The Hong Kong Polytechnic University (PolyU 152481/16E, PolyU 152110/17E) are acknowledged.

Appendix A: Discussion on the stress-free boundary condition for continuous film

For the case of continuous film on disk-like substrate, as the intrinsic strains of the film and substrate $\varepsilon_{\mathrm{f0}}$ and $\varepsilon_{\mathrm{s0}}$ represent their deformation at stress-free state, the interfacial stress should affect their deformation in an either positive or negative way, depending on the direction of the interfacial stress. Without loss of generality, we assume that $\varepsilon_{\mathrm{f0}} > \varepsilon_{\mathrm{s0}}$ or $\varepsilon_{\mathrm{mis}} \equiv \varepsilon_{\mathrm{f0}} - \varepsilon_{\mathrm{s0}} > 0$. Such strain misfit causes opposite shear tractions on the film and substrate as shown in Fig. 2(a), resulting in contracting and expanding additional displacements in the film and substrate, respectively. Since $\varepsilon_\theta = u_r/r$, we have $\varepsilon_{\mathrm{f0}} > \varepsilon_\theta^{(\mathrm{f})} = \varepsilon_\theta^{(\mathrm{s})} > \varepsilon_{\mathrm{s0}}$, which implies $\varepsilon_\theta^{(\mathrm{s})} - \varepsilon_{\mathrm{s0}} < \varepsilon_{\mathrm{f0}} - \varepsilon_{\mathrm{s0}} = \varepsilon_{\mathrm{mis}}$. Recalling Eq. (8), we have

$$0 < \frac{\tau_{\mathrm{de}}}{\varepsilon_{\mathrm{mis}}} < \frac{3E_{\mathrm{s}}t_{\mathrm{s}}}{(\nu_{\mathrm{s}}+2)(1-\nu_{\mathrm{s}})R} \tag{A1}$$

which unveils the implicit upper limit of the ratio of $\tau_{\mathrm{de}}/\varepsilon_{\mathrm{mis}}$ in our design. This limit also exists in the case with $\varepsilon_{\mathrm{f0}} < \varepsilon_{\mathrm{s0}}$. Eq. (A1) implies that $\sigma_r^{(\mathrm{f})}|_{r=R} \neq 0$, namely the boundary condition of Eq. (14) is unrealistic and can hardly be satisfied.

Appendix B: Discussion on the stress-free boundary condition for island film

For the case of island film on half-space substrate, we would examine whether the stress-free boundary condition in the film, i.e., $\sigma_r^{(\mathrm{f})}|_{r=R} = 0$, can be satisfied. We denote $\tilde{\varepsilon}_\theta^{(\mathrm{s})}$ as

$$\tilde{\varepsilon}_\theta^{(\mathrm{s})} = \frac{4\tau_{\mathrm{de}}(1-\nu_{\mathrm{s}}^{\,2})}{E_{\mathrm{s}}\pi} \cdot f(\bar{r}) \tag{B1}$$

where $f(\bar{r}) = \frac{1}{\bar{r}^2}\int_0^{\bar{r}} \frac{\lambda^2\left[\ln\left(1+\sqrt{1-\lambda^2}\right)-\ln\lambda\right]}{\sqrt{\bar{r}^2-\lambda^2}}\mathrm{d}\lambda$, $\bar{r} = r/R \in [0,1]$. Substituting Eq. (B1) into Eq. (19), we have

$$\sigma_r^{(\mathrm{f})} = \frac{E_{\mathrm{f}}}{1-\nu_{\mathrm{f}}} \cdot \left[\frac{4\tau_{\mathrm{de}}(1-\nu_{\mathrm{s}}^{\,2})}{E_{\mathrm{s}}\pi} \cdot f(\bar{r}) - \varepsilon_{\mathrm{mis}}\right] + \frac{4\tau_{\mathrm{de}}E_{\mathrm{f}}(1-\nu_{\mathrm{s}}^{\,2})}{E_{\mathrm{s}}\pi(1-\nu_{\mathrm{f}}^{\,2})} \cdot \bar{r}\frac{df(\bar{r})}{d\bar{r}}$$

Stress-free boundary condition requires $\sigma_r^{(\mathrm{f})}|_{\bar{r}=1} = 0$, that is, when $\bar{r} = 1$,

$$\frac{E_{\mathrm{f}}}{1-\nu_{\mathrm{f}}} \cdot \left[\frac{4\tau_{\mathrm{de}}(1-\nu_{\mathrm{s}}^{\,2})}{E_{\mathrm{s}}\pi} \cdot f(\bar{r}) - \varepsilon_{\mathrm{mis}}\right] + \frac{4\tau_{\mathrm{de}}E_{\mathrm{f}}(1-\nu_{\mathrm{s}}^{\,2})}{E_{\mathrm{s}}\pi(1-\nu_{\mathrm{f}}^{\,2})} \cdot \bar{r}\frac{df(\bar{r})}{d\bar{r}} = 0\,.$$

Further simplification gives

$$f(\bar{r}) + \frac{1}{1+\nu_{\mathrm{f}}} \cdot \bar{r}\frac{df(\bar{r})}{d\bar{r}} - \frac{\pi E_{\mathrm{s}}\varepsilon_{\mathrm{mis}}}{4\tau_{\mathrm{de}}(1-\nu_{\mathrm{s}}^{\,2})} = 0\,. \tag{B2}$$

Since $f(\bar{r}=1) \approx 0.416$, $\bar{r}\frac{df(\bar{r})}{d\bar{r}}|_{(\bar{r}\to 1)} \to -\infty$ and $\frac{\pi E_{\mathrm{s}}\varepsilon_{\mathrm{mis}}}{4\tau_{\mathrm{de}}(1-\nu_{\mathrm{s}}^{\,2})} > 0$, Eq. (B2) cannot be satisfied, namely, the stress-free boundary condition of $\sigma_r^{(\mathrm{f})} = 0$ at the edge (r=R) is unrealistic.

Appendix C: Linear approximation of the gradient thickness

For an island film on half-space substrate, the solution to the optimal gradient film thickness $t_{\mathrm{f}}(r)$ shown in Fig. 5(a) seems like a cone, which inspires us to look for the possible linear approximation of $t_{\mathrm{f}}(r)$ at least under some proper conditions.

Suppose the thickness profile function can be approximated by a linear function as

$$t_{\mathrm{f}}(r) = m(r - R) \tag{C1}$$

where R is the radius of the island film and m is the slope to be determined. Substituting Eq. (C1) into Eq. (20), we have

$$m = \frac{\tau_{\mathrm{de}}(1-\nu_{\mathrm{f}}{}^2)/E_{\mathrm{f}}}{(4r-3R)\cdot\dfrac{\partial\tilde{\varepsilon}_\theta^{(\mathrm{s})}}{\partial r} + r(r-R)\cdot\dfrac{\partial^2\tilde{\varepsilon}_\theta^{(\mathrm{s})}}{\partial r^2} + (1+\nu_{\mathrm{f}})\tilde{\varepsilon}_\theta^{(\mathrm{s})} - \varepsilon_{\mathrm{mis}}(1+\nu_{\mathrm{f}})} \tag{C2}$$

Inserting Eq. (B1) into Eq. (C2) to eliminate $\tilde{\varepsilon}_\theta^{(\mathrm{s})}$ gives

$$m = \frac{E_{\mathrm{s}}(1-\nu_{\mathrm{f}}{}^2)/E_{\mathrm{f}}(1-\nu_{\mathrm{s}}{}^2)}{g(\bar{r}) - \varphi} \tag{C3}$$

where

$$g(\bar{r}) = \frac{4}{\pi}\left[(1+\nu_{\mathrm{f}})f(\bar{r}) + (4\bar{r}-3)f'(\bar{r}) + \bar{r}(\bar{r}-1)f''(\bar{r})\right], \tag{C4}$$

$$f(\bar{r}) = \frac{1}{\bar{r}^2}\int_0^{\bar{r}} \frac{\lambda^2\cdot[\ln(1+\sqrt{1-\lambda^2}) - \ln\lambda]}{\sqrt{\bar{r}^2-\lambda^2}}\mathrm{d}\lambda\,, \tag{C5}$$

$$\varphi \equiv \frac{E_{\mathrm{s}}\varepsilon_{\mathrm{mis}}(1+\nu_{\mathrm{f}})}{\tau_{\mathrm{de}}(1-\nu_{\mathrm{s}}{}^2)}\,. \tag{C6}$$

Numerical integration was adopted to calculate $f(\bar{r})$ and $g(\bar{r})$ above. Fig. C1 shows the calculated variation of $g(\bar{r})$ with $\bar{r}$. As $\bar{r}$ varies from 0 to 1.0, it can be seen that function $g(\bar{r})$ takes finite value except in the vicinity of $\bar{r} = 0$. Further analysis indicated that as $\bar{r} \to 0$, $g(\bar{r})$ asymptotically approaches $2/\bar{r}$ which is also plotted in Fig. C1 for comparison. Considering that the Young's modulus of the substrate (E_{s}) is more than 4-5 orders of magnitude higher than the design shear stress (τ_{de}) and the strain mismatch $(\varepsilon_{\mathrm{mis}})$ is around a few percent, the value of φ in Eq. (C6) should be on the order of magnitude of 1000. In most of the region of $\bar{r} \in [0,1]$, $g(\bar{r}) \ll \varphi$ except in the vicinity of $\bar{r} = 0$. Therefore, m in Eq. (C3) can be approximated as a constant of $m \cong -\frac{\tau_{\mathrm{de}}(1-\nu_{\mathrm{f}})}{E_{\mathrm{f}}\varepsilon_{\mathrm{mis}}}$. Then the thickness profile can be approximated by a linear function as follows

$$t_{\mathrm{f}}(r) \cong \frac{\tau_{\mathrm{de}}(1-\nu_{\mathrm{f}})}{\varepsilon_{\mathrm{mis}} E_{\mathrm{f}}}(R-r). \tag{C7}$$

Eq. (C7) can be regarded as the approximate solution of $t_{\mathrm{f}}(r)$ as φ is large enough. The validity of this approximate solution was discussed in Section 2.2 for different φ.

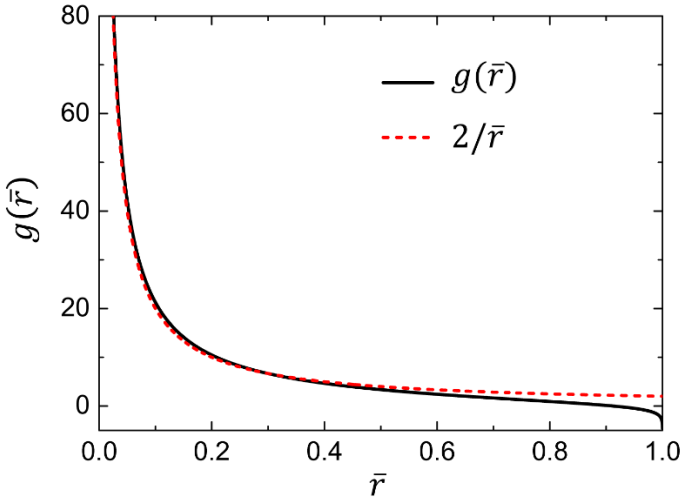

Fig. C1. Variation of $g(\bar{r})$ with $\bar{r}$ in comparison with its asymptotic form of $2/\bar{r}$. Here, the Poisson's ratio of the film is taken as $\nu_{\mathrm{f}} = 0.3$.

References

Akisanya, A., Fleck, N., 1997. Interfacial cracking from the freeedge of a long bi-material strip. International Journal of Solids and Structures 34, 1645-1665.

Antonyuk, V., Soroka, E., Lyashenko, B., Rutkovskii, A., 2007. Discontinuous coatings on cutting tools. Strength of Materials 39, 99-102.

Basu, S., Suresh, S., Ghatak, K., Bartolucci, S.F., Gupta, T., Hundekar, P., Kumar, R., Lu, T.-M., Datta, D., Shi, Y., 2018. Utilizing van der Waals slippery interfaces to enhance the electrochemical stability of Silicon film anodes in lithium-ion batteries. ACS Applied Materials & Interfaces 10, 13442-13451.

Blaber, J., Adair, B., Antoniou, A., 2015. Ncorr: open-source 2D digital image correlation matlab software. Experimental Mechanics 55, 1105-1122.

Bruet, B.J., Song, J., Boyce, M.C., Ortiz, C., 2008. Materials design principles of ancient fish armour. Nature Materials 7, 748.

Brun, M.K., Singh, R.N., 1988. Effect of thermal expansion mismatch and fiber coating on the fiber/matrix interfacial shear stress in ceramic matrix composites. Advanced Ceramic Materials;(USA) 3.

Chen, P.-Y., Schirer, J., Simpson, A., Nay, R., Lin, Y.-S., Yang, W., Lopez, M.I., Li, J., Olevsky, E.A., Meyers, M.A., 2012. Predation versus protection: fish teeth and scales evaluated by nanoindentation. Journal of Materials Research 27, 100-112.

Choi, S.R., Hutchinson, J.W., Evans, A.G., 1999. Delamination of multilayer thermal barrier coatings. Mechanics of Materials 31, 431-447.
Era, H., Otsubo, F., Uchida, T., Fukuda, S., Kishitake, K., 1998. A modified shear test for adhesion evaluation of thermal sprayed coating. Materials Science and Engineering: A 251, 166-172.
Gao, H., Wang, X., Yao, H., Gorb, S., Arzt, E., 2005. Mechanics of hierarchical adhesion structures of geckos. Mechanics of Materials 37, 275-285.
Gao, H., Yao, H., 2004. Shape insensitive optimal adhesion of nanoscale fibrillar structures. Proceedings of the National Academy of Sciences of the United States of America 101, 7851-7856.
Guo, Z., Zhou, L., Yao, H., 2019. Improving the electrochemical performance of Si-based anode via gradient Si concentration. Materials & Design, 107851.
Haftbaradaran, H., Soni, S.K., Sheldon, B.W., Xiao, X., Gao, H., 2012a. Modified stoney equation for patterned thin film electrodes on substrates in the presence of interfacial sliding. Journal of Applied Mechanics 79, 031018.
Haftbaradaran, H., Xiao, X., Verbrugge, M.W., Gao, H., 2012b. Method to deduce the critical size for interfacial delamination of patterned electrode structures and application to lithiation of thin-film silicon islands. Journal of Power Sources 206, 357-366.
Hein, V., Erdogan, F., 1971. Stress singularities in a two-material wedge. International Journal of Fracture Mechanics 7, 317-330.
Ingrole, A., Hao, A., Liang, R., 2017. Design and modeling of auxetic and hybrid honeycomb structures for in-plane property enhancement. Materials & Design 117, 72-83.
Jitcharoen, J., Padture, N.P., Giannakopoulos, A.E., Suresh, S., 1998. Hertzian-crack suppression in ceramics with elastic-modulus-graded surfaces. Journal of the American Ceramic Society 81, 2301-2308.
Johnson, K.L., 1987. Contact Mechanics. Cambridge University Press.
Kurniawan, R., Ko, T.J., 2013. A study of surface texturing using piezoelectric tool holder actuator on conventional CNC turning. International Journal of Precision Engineering and Manufacturing 14, 199-206.
Lee, Y., Erdogan, F., 1994. Residual/thermal stresses in FGM and laminated thermal barrier coatings. International Journal of Fracture 69, 145-165.
Pan, B., Qian, K., Xie, H., Asundi, A., 2009. Two-dimensional digital image correlation for in-plane displacement and strain measurement: a review. Measurement Science and Technology 20, 062001.
Pender, D., Padture, N., Giannakopoulos, A., Suresh, S., 2001. Gradients in elastic modulus for improved contact-damage resistance. Part I: The silicon nitride–oxynitride glass system. Acta Materialia 49, 3255-3262.
Piggott, M.R., 1997. Why interface testing by single-fibre methods can be misleading. Composites Science and Technology 57, 965-974.
Qin, F., Hu, J., Chou, Y.K., Thompson, R.G., 2009. Delamination wear of nano-diamond coated cutting tools in composite machining. Wear 267, 991-995.

Ramachandra, S., Ovaert, T.C., 2000. Effect of coating geometry on contact stresses in two-dimensional discontinuous coatings. Journal of Tribology 122, 665-671.
Rao, A., 1971. Stress concentrations and singularities at interface corners. ZAMM-Journal of Applied Mathematics and Mechanics/Zeitschrift für Angewandte Mathematik und Mechanik 51, 395-406.
Schaldach, M., Kranz, C., 2004. Stent having discontinuous coating in the form of coating islands. Google Patents.
Shenoy, V.B., Johari, P., Qi, Y., 2010. Elastic softening of amorphous and crystalline Li–Si phases with increasing Li concentration: a first-principles study. Journal of Power Sources 195, 6825-6830.
Soni, S.K., Sheldon, B.W., Xiao, X., Verbrugge, M.W., Dongjoon, A., Haftbaradaran, H., Gao, H., 2011. Stress mitigation during the lithiation of patterned amorphous Si islands. Journal of the Electrochemical Society 159, A38-A43.
Soroka, E., Lyashenko, B., Qiao, S., Zhang, C., 2011. Tribological behaviour and cutting performance of PVD-TiN coating/substrate system with discontinuous surface architecture. Rare Metal Materials and Engineering 40, 580-584.
Suresh, S., Olsson, M., Giannakopoulos, A., Padture, N., Jitcharoen, J., 1999. Engineering the resistance to sliding-contact damage through controlled gradients in elastic properties at contact surfaces. Acta Materialia 47, 3915-3926.
Valadez-Gonzalez, A., Cervantes-Uc, J.M., Olayo, R., Herrera-Franco, P.J., 1999. Effect of fiber surface treatment on the fiber–matrix bond strength of natural fiber reinforced composites. Composites Part B: Engineering 30, 309-320.
Vaßen, R., Giesen, S., Stöver, D., 2009. Lifetime of plasma-sprayed thermal barrier coatings: comparison of numerical and experimental results. Journal of Thermal Spray Technology 18, 835.
Volosova, M.A., Grigoriev, S.N., Ostrikov, E.A., 2016. Use of laser ablation for formation of discontinuous (discrete) wear-resistant coatings formed on solid carbide cutting tool by electron beam alloying and vacuum-arc deposition. Mechanics & Industry 17, 720.
Wang, C., Wang, Y., Fan, S., You, Y., Wang, L., Yang, C., Sun, X., Li, X., 2015. Optimized functionally graded $La_2Zr_2O_7$/8YSZ thermal barrier coatings fabricated by suspension plasma spraying. Journal of Alloys and Compounds 649, 1182-1190.
Xiao, X., Liu, P., Verbrugge, M., Haftbaradaran, H., Gao, H., 2011. Improved cycling stability of silicon thin film electrodes through patterning for high energy density lithium batteries. Journal of Power Sources 196, 1409-1416.
Yao, H., Dao, M., Imholt, T., Huang, J., Wheeler, K., Bonilla, A., Suresh, S., Ortiz, C., 2010. Protection mechanisms of the iron-plated armor of a deep-sea hydrothermal vent gastropod. Proceedings of the National Academy of Sciences of the United States of America 107, 987-992.
Yao, H., Gao, H., 2006. Optimal shapes for adhesive binding between two elastic bodies. Journal of Colloid and Interface Science 298, 564-572.
Yao, H., Gao, H., 2010. Gibson-soil-like materials achieve flaw-tolerant adhesion. Journal of Computational and Theoretical Nanoscience 7, 1299-1305.

Yu, H.-H., Hutchinson, J.W., 2003. Delamination of thin film strips. Thin Solid Films 423, 54-63.
Zhu, Y.L., Ma, S.N., Xu, B.S., 1999. Finite-element evaluation and improvement of a test procedure for coating shear bond strength determination. Journal of Thermal Spray Technology 8, 328-332.